Classification and spatial mapping of atmospheric corrosion of China

Yu Han（✉ hanyugeiri@163.com ）

  State Grid Smart Grid Research Institute Co.,Ltd.

Wenkui Hao

  State Grid Smart Grid Research Institute Co.,Ltd.

Lingling Xu

  DC Technical Center of State Grid Corporation of China

Xin Chen

  State Grid Smart Grid Research Institute Co.,Ltd.

Yan Jin

  State Grid Corporation of China

Xinghui Zhang

  State Grid Corporation of China

Yun Chen

  State Grid Smart Grid Research Institute Co.,Ltd.

Luyao Huang

  State Grid Smart Grid Research Institute Co.,Ltd.

Bingkun Yang

  State Grid Smart Grid Research Institute Co.,Ltd.

Zhixiang Zhu

  State Grid Smart Grid Research Institute Co.,Ltd.

Xiaofang Wang

  State Grid Smart Grid Research Institute Co.,Ltd.

Article

Abstract

Atmospheric corrosion is ubiquitous in China but varies a lot among different regions covering the cold, temperate and tropical zones. Categorizing the atmospheric corrosivity and plotting precise atmospheric corrosion map remain key interest for a variety of industries. The present work proposed an atmospheric corrosion map of China for hot-dip galvanized steels, which was constructed by inverse distance weighting (IDW) interpolation algorithm based on both the measured corrosion rates of coupons exposed at 2393 inland test stations and calculated corrosion rates from a prevalent dose-response function in 2918 sites in coastal regions. When the corrosion category was used as the criterion, the IDW interpolation algorithm of power 2 performed best. Cross-validation results confirmed that the prediction accuracy of IDW interpolation reached 85.6%. Based on the corrosion map, the categories of atmospheric corrosivity of China could be determined. The atmospheric corrosion map shows C2 (50.07%) and C3 (44.14%) zones cover the vast majority of China. C4-CX categories (highly corrosive regions) account for 4.07% (390760 km^2) of China.

Introduction

Atmospheric corrosion refers to a spontaneous degradation process of metals resulting from interactions with its surrounding environmental variables (e.g. relative humidity (RH) and temperature) and accumulative atmospheric contaminants (e.g. deposition of chlorides and sulfides), which is the most common type of corrosion that widely influences multiple industries such as infrastructure, transportation and manufacturing[1–3]. Atmospheric corrosion is estimated to account for more than half of all corrosion damages[4–5]. Quantifying the accurate area of different corrosion categories is an important step in raising awareness of the seriousness of corrosion issues, particularly relevant to decision makers in the industry and government—such that better policies can be established to improve our ability for mitigating corrosion risks in severe corrosion area. Differentiated materials selection and efficient corrosion protection based on corrosivity classification become a key to sustain integrity of the metallic facilities and equipment and reduce corrosion costs for different industries[6].

A precise atmospheric corrosion map provides an important guide to differentiated materials selection and economical engineering design since it enables a visual cue for the identification of atmospheric corrosion category and prediction of service life of metals and coatings in any given region. Plotted in the 1960s, the atmosphere corrosion map of the British Isles has been known as the pioneer trying to visualize the effect of atmospheric corrosion[7]. Subsequently, the atmospheric corrosion maps of different countries and cities, including Switzerland, Brazil, Spain, Korea, Slovakia, Thailand, Vietnam, Abu Dhabi and Istanbul have been drawn for the assessment of their atmospheric corrosion risks[8–16]. Plotting precise atmospheric corrosion map has been of great interest to corrosion scientists and engineers in China for many decades. Since the 1990s, China has conducted a number of differently scaled studies on the corrosion map in certain areas exposed to diverse corrosion environments[17]. Based on the corrosion data of carbon steel exposed in 20 corrosion sites, Wang et al. [18] drew the atmospheric corrosion map of Hainan province. Fan et al.[19] constructed an atmospheric corrosion map of Shandong province by using one year corrosion rate of hot-dip galvanized steel from 100 exposure corrosion test sites. Huang et al.[20] collected a set of corrosion data of Q235 steel from 48 sites and drew an atmospheric corrosion map of Guangdong province, China. However, a nationwide atmospheric corrosion map is lacked for a long time in consideration of vast territory and diverse climates in China.

The biggest challenge in corrosion map optimization is how to improve the accuracy of the map so that to provide local corrosion data with high precision. The accuracy of the map is firstly supported by plenty of corrosion data derived from sufficient on-site atmospheric exposure sites. On the basis of one year on-site exposure tests at 21 sites both in marine and urban regions, Kim et al.[21] constructed an atmospheric corrosion map of Korea. Vera et al.[22] collected the corrosion data of carbon steel and galvanized steel after one-year exposure in 31 stations in Chile and developed a national map

of corrosion. Kumar et al.[23] constructed an atmospheric corrosion map of India by collecting corrosion data in 32 stations consecutively. However, by considering the vast territory and climate changes in these countries, such a scale of corrosion sites is not able to meet the demand of drawing a corrosion map with high resolution. Also, on-site exposure corrosion tests are usually established in urban area to reduce the manpower and the cost of corrosion data collection. Less exposure sites were set up in rural area and natural environments, where large infrastructure construction, like power lines and high speed railway, suffer from serious corrosion and deterioration. The accurate corrosion categories in these regions face challenges. To better predict the atmospheric corrosion in these regions, different statistical or parametric models regarding corrosion prediction in correlation with environmental factors were proposed based on long-term atmospheric environmental metal corrosion tests[24,25]. They include dose response functions (DRFs), developed for several common metals based on regression analysis that have been used for the prediction of atmospheric corrosion rate of metals[26-28]. DFRs are currently more popular since they are simpler and do not require large-scale outdoor exposure tests to obtain corrosion data[29]. ISO 9223 recommends a DRF to predict first-year corrosion rate of four typical metals, including carbon steel, zine, copper, and aluminum, based on temperature, RH, chloride deposition rate, and sulfur dioxide deposition rate[30]. Based on this, some researchers introduced more environmental parameters into the power function and proposed more sophisticated DRFs regarding corrosion prediction. The UN/ECE ICP Materials project proposed a set of DRFs described with RH, temperature, sulfur dioxide, nitrogen dioxide, ozone, rainfall, rainfall acidity, and particulate matter, which is suitable for mapping and calculations of cost of corrosion damage[31]. However, the prediction accuracy of DRFs in different climates varies largely. Castañeda et al.[25] prososed that the DRFs of ISO 9223 may over estimate corrosion rate in tropical region and under estimate corrosion rate in Asia region. The prediction accuracy of the corrosion map may be reduced sharply when large corrosion data from DRFs are used in interpolation calculation.

In the mapping process, interpolation techniques such as inverse distance weighting (IDW) interpolation algorithm have been applied in atmosphere corrosion. IDW is a deterministic method, which assumes that the value of the point decreases in weight or influence as it increases in distance from that point[32]. The power parameter within the IDW tool controls the weight of individual points, which can be used to increase the accuracy of the interpolation method. However, the validity of the interpolation algorithm were not discussed[33,34]. This study attempted to draw a precise atmospheric corrosion map of China to provide guidance to corrosion mitigation of industrial engineering. One year on-site exposure tests was firstly carried out using hot-dip galvanized steel at 2393 stations in China. Chloride distribution equation was also proposed to better predict corrosion rate along coastal area by using the DRFs presented in ISO 9223. Based on this, an optimized atmospheric corrosion map of the study area was drawn by IDW interpolation algorithm. After running the interpolations, a cross validation was performed on each of the predicted surfaces. To the best of our knowledge, this work is the first report providing nationwide category of atmospheric corrosivity, which will strongly support the differentiated materials selection and efficient corrosion protection in China.

Results And Discussion

Category of corrosivity of atmosphere in China

ISO 9223 standard recommends a classification of the corrosivity of the atmospheric environments by dividing the one-year corrosion rate data of typical metal materials obtained from on-site atmospheric exposure sites into six categories, from low to high, are C1, C2, C3, C4, C5, and CX, respectively. In this study, the corrosion of galvanized steel sample in the first year can be considered as the corrosion of zinc. The distribution of the test stations are presented in Fig. 1 and the corresponding corrosion categories of carbon steel is shown in Fig. 2. More than 85% of the corrosion exposure stations (i.e., 2034 stations) are located in mild corrosion zones, among which C2 accounts for 44.24% of the total, C3 is

41.11% and C1 is only 2.64%. C4, C5 and CX represent relatively high corrosion rates. About one-tenth of the corrosion exposure stations lies on C4 area and 1.79% in C5 area. Notably, about 1% of the corrosion exposure stations are located in CX region, which are considered as extreme corrosion risk.

More specifically, the corrosion categories of galvanized steel in different provinces of China are shown in Fig. 3. According to geographical and climatic differences, these provinces are divided into six parts, Northwest China, Southwest China, Northeast China, North China, Central China, Eastern China and South China. The corrosion category distribution of the exposure stations appears some regularity in spite of its variation in various province. The proportion of exposure stations in heavily corroded area (C4 and above) gradually increased from the northwest to the southeast of China. Except for Xinjiang province, most stations are located in C2 area in the five provinces Northwest, suggesting a relatively mild corrosion risk. C3 category occupied almost 70% of the stations in Xinjiang province, which may be attributed to the huge difference of geography conditions. Most of the stations are located in humid climate regions, where human activities and industrial production occurs (Fig. 1b). In Southwest China, more than 90% of stations are located in C3 category in Chongqing municipality, while more slight corrosion categories were observed in Tibet and Sichuan province. High relative humidity and abundant rainfall account for the increased corrosion risk in Chongqing municipality. As for Tibet, more stations are needed to enrich the essential corrosion data and determine a more precise corrosion categories. In North China, notably, a significant increase of station numbers of C4 categories was observed in Shanxi and Hebei provinces compared the other 3 provinces, which is because the large number for coal mines that lead to a higher concentration of pollutants in the atmosphere in this area. The most severe corrosion risk was observed in Eastern China and South China, especially in coastal regions in Zhejiang, Fujian, Guangdong, Guangxi, Hainan and Taiwan, where more than 50% of stations located in C4-CX categories, suggesting that a comprehensive corrosion protection is urgently needed to the application, operation and maintenance of metal materials.

Chloride ion diffusion model in coastal region

Table 1 shows the deposition rate of chloride for environment monitor station along the distance to the coastline. Average chloride deposition rates collected monthly over one year were plotted as a function of distance to the sea as shown in Fig. 4a. Chloride deposition rate is the highest at the shore and sharply decreases within 1 km from the shoreline (Fig. 4b). At the distance > 1 km, the decay is gradually decreasing. Significantly, the increase of chloride deposition rate at 8 km can be attributed to the fact that the diffusion of chloride ions was blocked by buildings, trees, and shelters[13]. Based on these data, a chloride ion diffusion model in coastal region is proposed as followed:

$$y = 48.547 \cdot x^{-0.376}, R^2 = 0.920 \quad (1)$$

wherein x and y are the distance to the sea and chloride ion deposition rate, respectively. In this study, 2918 sites in coastal provinces were selected to calculate their chloride ion deposition rates according to the above equation.

Table 1
The deposition rate of chloride for environment monitor station along the distance to the coastline.

Station number	1	2	3	4	5	6	7	8
Distance to the coastline(km)	0.01	0.1	1.7	4	7	8	15	30
Deposition rate of chloride $(mg/(m^2 \cdot d))$	195	98.37	58.14	21.54	33.13	31.16	14.65	8.22

Dose-response function in coastal region

Metals are exposed to hundreds of times more chloride in coastal region than that inland, which lead to severe corrosion of metals and further major insecurity of infrastructures. Due to the limitation of the field tests, the corrosion exposure data are insufficient in coastal region, especially for test sites within 0−1 km from the coastline, which leads to inaccuracy of corrosion category estimation. To solve this problem, a DRF recommended by ISO 9223, incorporating chloride deposition rate, sulfur dioxide deposition rate, temperature and RH, was used to evaluate the corrosivity within 0−30 km from the coastline. Combined with the measured corrosion data in 2393 inland stations, the calculated corrosion data participate in the interpolation to improve the accuracy of the corrosion map. The equation for zinc is expressed as:

$$r_{corr}=0.0129 \bullet P_d^{0.44} \bullet \exp\left(0.046\bullet RH + f_{Zn}\right) + 0.0175 \bullet S_d^{0.57} \bullet \exp\left(0.008 \bullet RH + 0.085 \bullet T\right)$$

2

$$f_{Zn} = 0.038 \bullet (T-10) \ \ T \leq 10 \ ^{\circ}C \ \ f_{Zn} = -0.071 \bullet (T-10) \ \ T > 10 \ ^{\circ}C$$

where r_{corr} is first-year corrosion rate of zinc (μm/a); P_d and S_d are the annual average SO_2 deposition and annual average Cl^- deposition (mg·m^{-2}·d^{-1}), respectively; T and RH represent the annual average temperature (ºC) and relative humidity (%), respectively; f_{Zn} is a correlation coefficient of Zn. Combining the average temperature, RH provided by local meteorological department and observed sulfur dioxide deposition rate in coastal stations, the corrosion rates of zinc in 2918 coastal points were calculated, together with the observed corrosion rates inland, to serve as interpolation data.

Atmospheric corrosion map of China

Based on the first year corrosion rate (μm/a) of galvanized steel obtained from 2393 exposure test sites and calculated corrosion rates from a prevalent DRF in 2918 sites in coastal regions, the atmospheric corrosion map of China was construct by using the IDW spatial interpolation method.

Figure 5 shows the atmospheric corrosion maps obtained by IDW spatial interpolation method with powers of 1, 2, 3, and 4. The search radius was flexible with nearest 10 points participating in interpolation calculation. The distribution of corrosivity categories is consistent with different powers, that is, the corrosivity of the atmosphere in the coastal region is significantly higher than that in the inland region, which is consistent with the actual observed data.

After running the interpolations, a cross validation was performed on 700 points selected from different provinces. It compares measured values with the predicted ones from the predicted surface. The mean relative error (MRE), mean absolute error (MAE) and root-mean-square error (RMSE) of interpolation results are shown in Table 2. With the increasing of power values, the MRE, MAE and RMSE decreased at first and then increased, suggesting that IDW interpolation algorithm of power 2 performed best in the prediction of corrosion rate. The average MRE was the smallest with a value with 25.74% when the power was 2, which is reasonable on the basis that the study area covers more than 9.6 million square kilometers. The average MAE and RMSE of the interpolation results in the presence of power 2 were 0.2414 and 0.3018, respectively. All the three cross validation methods suggested that the power parameter of IDW interpolation algorithm is reasonable to ensure the accuracy of the interpolation method.

Table 2
The MRE, MAE and RMSE of interpolation results by cross validation.

P value	Numbers of stations	MRE (%)	MAE (μm/a)	RMSE (μm/a)
1	700	27.23	0.272	0.331
2	700	25.74	0.241	0.302
3	700	28.15	0.245	0.354
4	700	30.12	0.265	0.361

In main industrial sectors, like infrastructure, energy, transportation and manufacturing, corrosion scientists and engineers focus principally on the atmospheric corrosion category rather than the accurate corrosion rate in the project location. Thus, counting the accuracy of atmospheric corrosion category through cross validation should be considered a more important reference. The predicted corrosion rates in the extracted points were compared with measured corrosion rates in those stations and the result is shown in Table 3. Based on the prediction results, the atmospheric corrosion categories of 575 sites are consistent with the observed results, suggesting a prediction accuracy of 82.1% in the presence of power 1. The atmospheric corrosion categories of 93 stations are 1 grade different (higher or lower) compared with the corrosion categories calculated from those stations. Only 26 stations showed a 2 grades difference of the corrosion categories, which mainly impacted by long distance and local contamination in the surrounding sites. The IDW of power 2 performed best. The predicted atmospheric corrosion categories of 599 sites are consistent with observed results. Only 10.7% and 3.7% of sites showed a difference of 1 and 2 corrosion categories, respectively. As for the power 3 and 4, there are 83% and 80.4% of the calculated sites presented a same atmospheric corrosion category compared with the observed stations.

Table 3
Statistics of sites corrosion categories prediction results by cross validation.

	Power = 1		Power = 2		Power = 3		Power = 4	
	Numbers	Proportion (%)	Numbers	Proportion (%)	Numbers	Proportion (%)	Numbers	Proportion (%)
Consistent category	575	82.1%	599	85.6%	581	83%	563	80.4%
One category difference	93	13.3%	75	10.7%	95	13.6%	101	14.4%
Two categories difference	32	4.6%	26	3.7%	24	3.4%	36	5.2%

The corresponding area and proportion of different corrosion categories with power 2 are listed in Table 4. The vast majority of the studied area, with proportions of 50.07% and 44.14%, are lies on C2 and C3 areas staining with green and yellow, respectively. C2 occurs more in Southwest China and Northeast China, whereas C3 is more likely to appear in Northwest China and Eastern China. In addition, it was estimated that the C1 category (very low) mainly exist in Xizang, western Sichuan and Ningxia provinces, accounting for only 1.72% of study area. C4-CX categories account for only 4.07% (390,760 km^2) of the study area, which display cluster distribution in south and southeast coastal provinces including Zhejiang, Fujian Guangdong, Guangxi, Hainan, Taiwan and patchy distribution in inland provinces like Shanxi, Hebei and Hubei. Notably, though only 0.34% and 0.12% is dedicated to C5 and CX areas, respectively, a mass of metallic facilities and equipment served in infrastructure, transportation, manufacturing and public services face a

dramatically increased corrosion risk on the basis that C5 and CX areas are precisely where the most economically developed regions in China.

Table 4
The area and proportion of different corrosion categories.

Corrosion category	Area (km^2)	Proportion (%)
C1	165 140	1.72
C2	4 807 220	50.07
C3	4 236 880	44.14
C4	346 600	3.61
C5	32640	0.34
CX	11520	0.12

In summary, a precise atmospheric corrosion map of China was plotted by using IDW interpolation algorithm in this study. Both the measured corrosion rates of hot-dip galvanized steel coupons exposed in 2393 test stations inland and calculated corrosion rates from a prevalent DRF in 2918 sites in coastal regions were employed to construct the map. The precision of IDW interpolation algorithm was evaluated by cross validation. The important findings include:

1. A chloride ion diffusion model in coastal region is proposed. Chloride deposition rate decreases exponentially with increasing distance from the sea.
2. The atmospheric corrosion map shows C2 (50.07%) and C3 (44.14%) zones cover the vast majority of the study area. C4-CX categories account for 4.07% (390760 km^2) of the study area in China.
3. Cross-validation results demonstrated that the prediction accuracy of IDW interpolation algorithm was 85.6%
4. The atmospheric corrosion map of the study area can be used to improve our capacity for corrosion protection, operation maintenance, and life prediction for outdoor engineering materials in severe corrosion area.

Methods

Exposed materials and methods

Hot-dip galvanized steel coupons with dimensions of 150 × 70 × 3 mm^3 were used in this study. Coupons were all numbered and ultrasonically rinsed with deionized water and ethanol for 15 min (for 15 min in each solution). Before the expose test, the initial weights of the cleaned coupons were recorded by an electronic balance (Me 204, Mettler Toledo, precision ± 0.1 mg). The samples were mounted on shelves with the lowest position at 1 m above the ground, facing south with a slant angle of 45°. After one-year exposure tests, all the coupons were retrieved at each test station and the corrosion products were removed guided by ISO 9226[35]. The corrosion rate (r_{corr}) of each coupon was calculated using the following Eq. 3[6]:

$$r_{rorr} = \frac{3.65 \times 10^3 \times (w_0 - w_t)}{s \times t \times d}$$

3

where r_{corr} is the corrosion rate, expressed in grams per square meter per year (g/[m²·a]); w_0 and w_t represent the weights before and after the test, expressed in gram (g); s, t and d stand for the sample area expressed in square meter (m²), test time expressed in year (a) and material density expressed in grams per cubic centimeter (g/cm³). Triplicate samples were used for each test station to ensure the reproducibility of the results.

Atmospheric on-site exposure test

Atmospheric on-site exposure tests were conducted at 2393 corrosion test stations in China. Part of corrosion data were collected from literatures[20]. The details and geographical position distribution of the test stations are presented in Fig. 1. Three key principles were proposed in the optimized selection of test stations, including uniform distribution principle to ensure at least one station in every 1000 ~ 1500 km², moderate increase of the number of test stations in heavy corrosion environments and emphasis on differentiated environments and climate.

Environmental parameters collection

In coastal region, relevant environmental parameters including temperature, RH, chloride ion deposition rate and sulfur dioxide deposition rate were collected at different distances to the coastline. The weather data were obtained from the Meteorological Department data during the exposure test. Sulfur dioxide deposition was collected by PbO_2 cylinder method recommended by ISO 9225[37]. Particularly, Chloride ion deposition rate was measured by dry gauze method along the vertical direction of coastline in Fujian province. Table 1 shows the distance from the coastline for the collection sites. Double-layered dry gauze was fixed by a plastic frame with a diameter of 120 mm under the shelter of a perspex hood with the exposure orientation always facing the coastline. After monthly exposure, dry gauzes were extracted from exposure racks and were analyzed to obtain the chloride ion deposition rate guided by ISO 9225. Based on the results, a modified chloride ion diffusion model in coastal region of China was proposed. Finally, the corrosion rate was calculated via the DRF proposed by ISO 9223 from a 30-kilometer area around the coastline.

Atmospheric corrosion map

According to ISO 9223, the atmospheric corrosion can be divided into 6 categories from very low to extreme: C1, C2, C3, C4, C5, and CX. Based on the measured corrosion rate of hot-dip galvanized steel coupons exposed in 2393 test stations inland and calculated corrosion rate from DRF in 2918 sites around the coastline, in this work, the atmospheric corrosivity categories of these stations of China were determined.

To visualize the atmospheric corrosion map, the data of the collected cities were linked to their corresponding geographical coordinates and translated into colors on a map through ArcGIS software (version 10.4). Firstly, the longitudes and latitudes of the stations were put into ArcGIS software to mark out their corresponding locations on the map of China. Secondly, the corrosion rates of the stations were given to corresponding locations. Then the presented values of the whole country are computed based on IDW interpolation algorithm. To improve the accuracy of atmospheric corrosivity map and optimize visual experience, each category was divided into several sub-categories dyed with similar color scheme.

IDW interpolation algorithm explicitly works on the assumption that things which are closer to each other are more alike than those which are farther apart[38]. The interpolated values are essentially estimated by the local weighted averages, as shown in formulas (3) and (4):

$$Z_0 = \sum_{i=1}^{n} Z_i \lambda_i$$

3

$$\lambda_i = \frac{\frac{1}{d^p}}{\sum_{i=1}^{n} \frac{1}{d_i^p}}$$

4

in which Z_0 and Z_i are the estimated value at a predicted point and the observed value at a given point, respectively; λ_i is the weight value, which is a positive real number; n represents the number of sampled points used for the estimation. Greater values of p grant greater influence on values which are closest to the point to be interpolated[39]. The parameter prediction for the target location is a summation of the product of 'allotted weights' and 'measured values' for all sites. After reviewing numerous literature, p is taken to be 1–4 for the current study to optimize the atmospheric corrosion map.

Cross Validation

Cross validation was carried out in 700 stations in China to evaluate the performance of IDW interpolation algorithm. After extracted from the interpolation, the predicted corrsion rate is estimated by the observed data obtained from the closest 10 stations[40]. Then the predicted corrsion rate is compared with the extracted data. Both the corrosion rate and corrosion category of 700 stations and the results can be statistically analyzed. Three statistical methods were employed in this study include MAE (Eq. (5)), MRE (Eq. (6)), and RMSE (Eq. (7)), respectively.

$$MAE = \frac{1}{n} \sum_{i=1}^{n} |Z_i\text{-}Z_0|$$

6

$$MRE = \frac{1}{n} \sum_{i=1}^{n} \frac{|Z_i\text{-}Z_0|}{Z_i}$$

7

$$MRSE = \sqrt{\frac{1}{n} \sum_{i=1}^{n} (Z_i\text{-}Z_0)^2}$$

8

where Z_0 and Z_i are the predicted corrosion rate and the corresponding observed corrosion rate at point *i* at the same point, respectively. The smaller the values of MAE, MRE, and MRSE, the higher the interpolation precision.

Declarations

Date availability

The data presented in this article is available upon request to the authors.

ACKNOWLEDGEMENTS

Author information

Affiliations

China State Key Laboratory of Advanced Power Transmission Technology, State Grid Smart Grid Research Institute Co.,Ltd. 102209, Beijing, China.

Wenkui Hao, Xin Chen, Yu Han, Yun Chen, Luyao Huang, Bingkun Yang, Zhixiang Zhu, Xiaofang Wang

DC Technical Center of State Grid Corporation of China, Beijing, 100053, China.

Lingling Xu

State Grid Corporation of China, Beijing, 100032, China.

Yan Jin, Xinghui Zhang

Contributions

W.K.H. designed the experiments, analyzed the results, and wrote the paper. L.L.X., X.C., Y.J. and X.H.Z. contributed to the outdoor corrosion tests. Y.C., B.K.Y., Z.X.Z. and X.F.W. were responsible for data processing. Y.H. and L.Y.H. revised the paper. All the authors contributed to the interpretation of the experimental data.

Corresponding authors

Correspondence to Yu Han or Luyao Huang.

Ethics declarations

Competing interests

The authors declare no competing interests.

References

1. Koushik, B.G., Steen, N.V., Mamme, M.H., Ingelgem, Y.V. & Terryn, H. Review on modelling of corrosion under droplet electrolyte for predicting atmospheric corrosion rate. Journal of Materials Science & Technology **62**, 254–267 (2021).

2. Roberge, P.R., Klassen, R.D. & Haberecht, P.W. Atmospheric corrosivity modeling — a review. Materials & Design **23**, 321–330 (2002).

3. Lebozec, N., Jönsson, M. & Thierry, D. Atmospheric corrosion of magnesium alloys: influence of temperature, relative humidity, and chloride deposition. Corrosion **60**, 356–361 (2004).

4. Hou, B.R., Li, X.G., Ma, X.M., Du, C.W., Zhang, D.W., Zheng, M., Xu, W.C., Lu, D.Z. & Ma, F.B., The cost of corrosion in China. npj materials degradation **1**, 4 (2017).

5. Kumar, V., Sharma, N., Tiwari, S.K. & Kango, S., Atmospheric corrosion of materials and their effects on mechanical properties: A brief review. *Materials Today: Proceedings* **44**, 4677–4681 (2021).

6. Zhi, Y.J., Yang, T. & Fu, D.M., An improved deep forest model for forecast the outdoor atmospheric corrosion rate of low-alloy steels. Journal of Materials Science & Technology **49**, 202–210 (2020).

7. Shaw, T. R., Corrosion Map of the British Isles, In *Atmospheric Factors Affecting the Corrosion of Engineering Metals*. ASTM International **6464**, 204–215 (1978).

8. Reiss, D., Rihm, B., Thöni, C. & Faller, M. Mapping stock at risk and release of zinc and copper in Switzerland-dose response functions for runoff rates derived from corrosion rate data. Water Air, and Soil Pollution **159**, 101–113 (2004).

9. Sica, Y.C., Kenny, E.D., Portella, K.F. & Campos Filho, D.F. Atmospheric Corrosion Performance of Carbon Steel, Galvanized Steel, Aluminum and Copper in the North Brazilian Coast. Journal of the Brazilian Chemical Society **18**, 153–166 (2007).

10. Chico, B., Fuente, D., Vega, J.M., & Morcillo, M. Corrosivity maps of Spain for zinc in rural atmospheres. Revista de Metalurgia **46**, 485–492 (2010).

11. Kim, Y. S., Lim, H. K., Kim, J. J. & Park, Y.S. Corrosivity of Atmospheres in the Korean Peninsula. Corrosion Science and Technology **10**, 109–117 (2011).

12. Ivaskova, M., Kotes, P. & Brodnan, M. Air pollution as an important factor in construction materials deterioration in Slovak Republic. Procedia Engineering **108**, 131–138 (2015).

13. Pongsaksawad, W., Klomjit, P., Khamsuk, P., Sorachot, S. & Pålsson, N. S. Chloride distribution model and corrosion map of structural steels for tropical climate in Thailand. Science of the Total Environment **787**, 147465 (2021).

14. Ganther, W. D., Cole, I. S., Helal, A. M., Chan, W., Paterson, D. A., Trinidad, G., Corrigan, P., Mohamed, R., Sabah, N. & Al-Mazrouei, A. Towards the development of a corrosion map for Abu Dhabi. Materials and Corrosion **62**, 1066–1073 (2011).

15. Karaca, F., Mapping the corrosion impact of air pollution on the historical peninsula of Istanbul. Journal of Cultural Heritage 14, 129–137 (2013).

16. Cole, I., Corrigan, P. & Hue, N.V. Steel Corrosion Map of Vietnam. Corrosion Science and Technology **11**, 103–107 (2012).

17. Wu, D.Q., Zhang, D.W., Liu, S.P., Jin, Z.H., Chowwanonthapunyac, T., Gao, J. & Li, X.G. Prediction of polycarbonate degradation in natural atmospheric environment of China based on BP-ANN model with screened environmental factors. Chemical Engineering Journal **399**, 125878 (2020).

18. Wang, Z.Y., Chen, H.C., Yu, G.C. & Han, W. Investigation on Atmospheric Corrosiveness in Hainan Province. Journal of Iron and Steel Research International **10**, 59–62 (2003).

19. Fan, Z.B., Li, X.G., Jiang, B., Wang, X.M. & Wang, Q. Mapping Atmospheric Corrosivity in Shandong, Water Air, and Soil Pollution **231**, 569 (2020).

20. Huang, J.C., Meng, X.B., Zheng, Z.J. & Gao, Y. Optimization of the atmospheric corrosivity mapping of Guangdong Province. Materials and Corrosion **70**, 91–101 (2019).

21. Kim, Y. S., Lim, H. K., Kim, J. J., Hwang, W.S. & Park, Y.S. Corrosion Cost and Corrosion Map of Korea – Based on the Data from 2005 to 2010. Corrosion Science and Technology **10**, 52–59 (2011).

22. Vera, R., Puentes, M., Araya, R., Rojas, P. & Carvajal, A. Atmospheric corrosion map of Chile: results after one year of exposure. Revista De La Construccion **11**, 61–72 (2012).

23. Kumar, V. & Sil, A. Rubric Assessment and Spatial Zonal Mapping of Atmospheric Corrosion of Steel in India. Corrosion **77**, 795–808 (2021).

24. Tidblad, J., Kucera, V., Mikhailov, A.A., Henriksen, J., Kreislova, K., Yates, T., Stöckle, B. & Schreiner, M., UN ECE ICP Materials: dose-response functions on dry and wet acid deposition effects after 8 years of exposure, Water, Air, and Soil Pollution **130**, 1457–1462 (2001).

25. Castañeda, A. A., Corvo, F., Fernández, D. & Valdés, C. Outdoor-Indoor Atmospheric Corrosion in a Coastal Wind Farm Located in a Tropical Island. Engineering Journal **21**, 43–62 (2017).

26. Benarie, M. & Lipfert, F.L. A general corrosion function in terms of atmospheric pollutant concentrations and rain pH. Atmospheric Environment **20**, 1947–1958 (1986).

27. Panchenko, Y.M., Marshakov, A.I., Nikolaeva, L.A., Kovtanyuk, V.V., Igonin, T.N. & Andryushchenko, T.A. Comparative estimation of long-term predictions of corrosion losses for carbon steel and zinc using various models for the Russian territory. Corrosion Engineering, Science and Technology **52**, 149–157 (2017).

28. Zhi, Y.J., Jin, Z.H., Lu, L., Yang, T., Zhou, D.Y., Pei, Z.B., Wu, D.Q., Fu, D.M., Zhang, D.W. & Li, X.G. Improving atmospheric corrosion prediction through key environmental factor identification by random forest-based model. Corrosion Science **178**, 109084 (2021).

29. Mikhailov A.A. Estimating and Mapping the Material Corrosion Losses in the European Part of Russia with Unified Doze—Response Functions. Protection of Metals **38**, 281–296 (2002).

30. ISO 9223, 2012. Corrosion of metals and alloys – Corrosivity of atmospheres – Classification, determination and estimation.

31. Kucera, V., Tidblad. J., Kreislova, K., Knotkova, D., Faller, M., Reiss, D., Snethlage, R., Yates, T., Henriksen, J., Schreiner, M., Melcher, M., Ferm, M., Lefèvre, R. & Kobus, J. UN/ECE ICP Materials Dose-response Functions for the Multi-pollutant Situation. Water, Air, and Soil Pollution **7**, 249–258 (2007).

32. Castillo-Miranda, J. O. & Rodriguez-Gomez, F. J. Mapping of the cost of atmospheric corrosion of zinc and galvanised steel due to the effect of atmospheric pollution in the Mexico City Metropolitan area. Corrosion Engineering Science and Technology **57**, 408–419(2022).

33. Omran, E.S. E. Improving the Prediction Accuracy of Soil Mapping through Geostatistics. International Journal of Geosciences **3**, 574–590 (2012).

34. Kambezidis, H. D., & Kalliampakos, G., Mapping atmospheric corrosion on modern materials in the Greater Athens area. Water, Air, and Soil Pollution **224**, 1463 (2013).

35. ISO 9226, 2012. Corrosion of metals and alloys – Corrosivity of atmospheres – Determination of corrosion rate of standard specimens for the evaluation of corrosivity.

36. Hai, C., Wang, Z.G., Lu, F.Y., Zhang, S.P., Du, C.W., Cheng, X.Q. & Li, X.G. Analysis of Corrosion Evolution in Carbon Steel in the Subtropical Atmospheric Environment of Sichuan. Journal of Materials Engineering and Performance **22**, (2021).

37. ISO 9225, 2012. Corrosion of metals and alloys – Corrosivity of atmospheres – Determination of corrosion rate of standard specimens for the evaluation of corrosivity.

38. Lu, G.Y. & Wong D.W. An adaptive inverse-distance weighting spatial interpolation technique. Computers & Geosciences 34, 1044–1055 (2008).

39. Shukla, K., Kumar, P., Mann, G.S. & Khare, M. Mapping spatial distribution of particulate matter using Kriging and Inverse Distance Weighting at supersites of megacity Delhi. Sustainable Cities and Society **54**, 101997 (2020).

40. Denby, B., Sundvor, I., Cassiani, M., Smet, P., Leeuw, F. & Horálek, J. Spatial mapping of ozone and SO_2 trends in Europe. Science of the Total Environment **408**, 4795–4806 (2010).
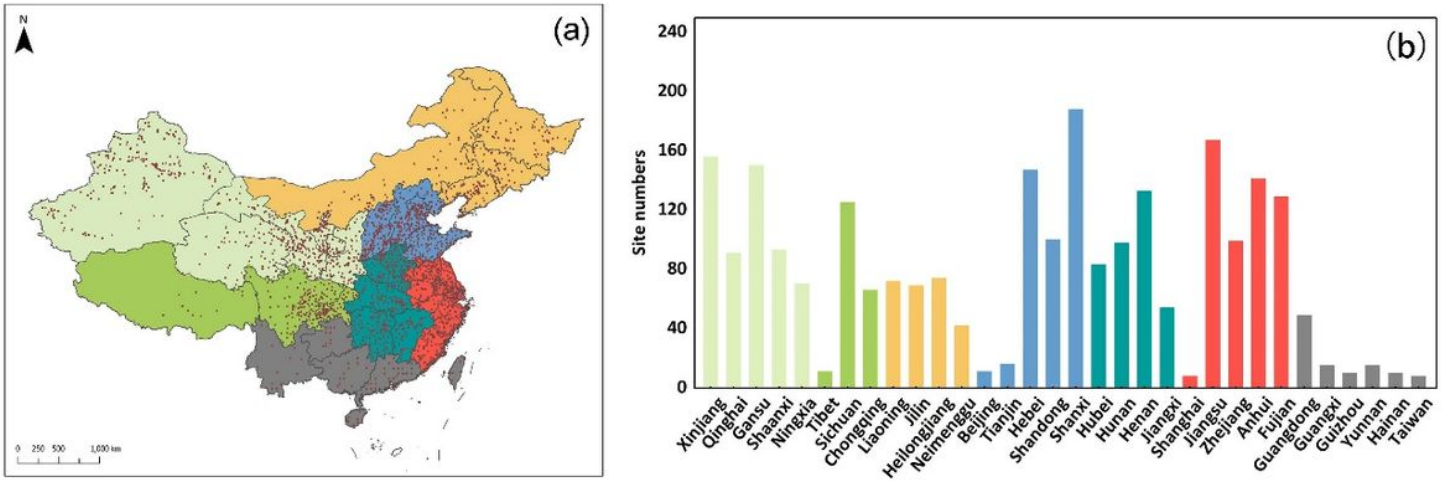
Figures

Figure 1

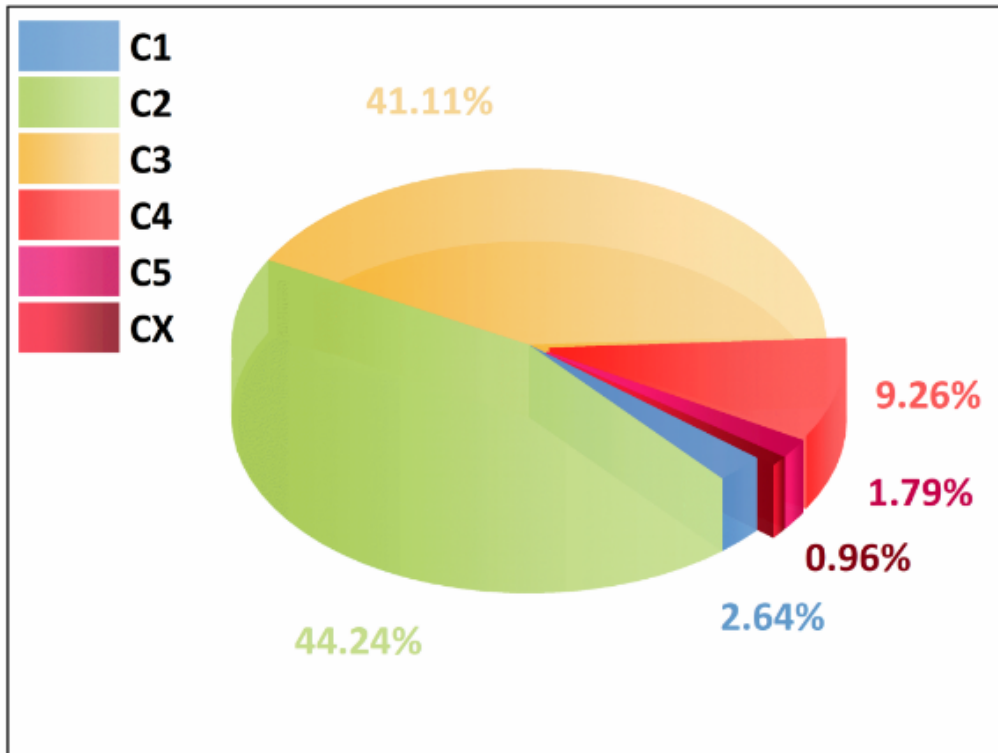The distribution and amount of 2393 exposure corrosion stations in China.

Figure 2

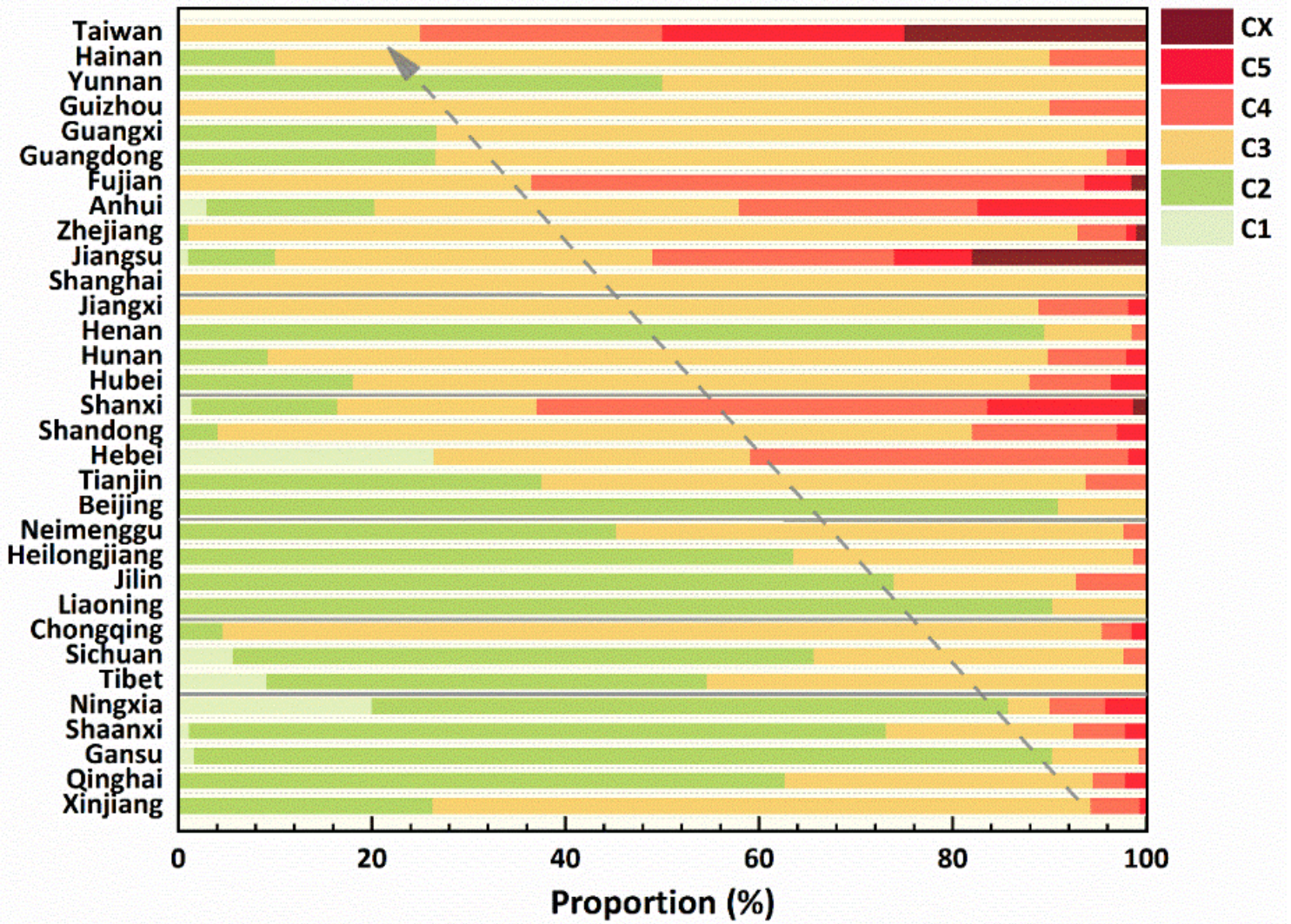Results of corrosion categories of galvanized steel according to ISO 9223.

Figure 3

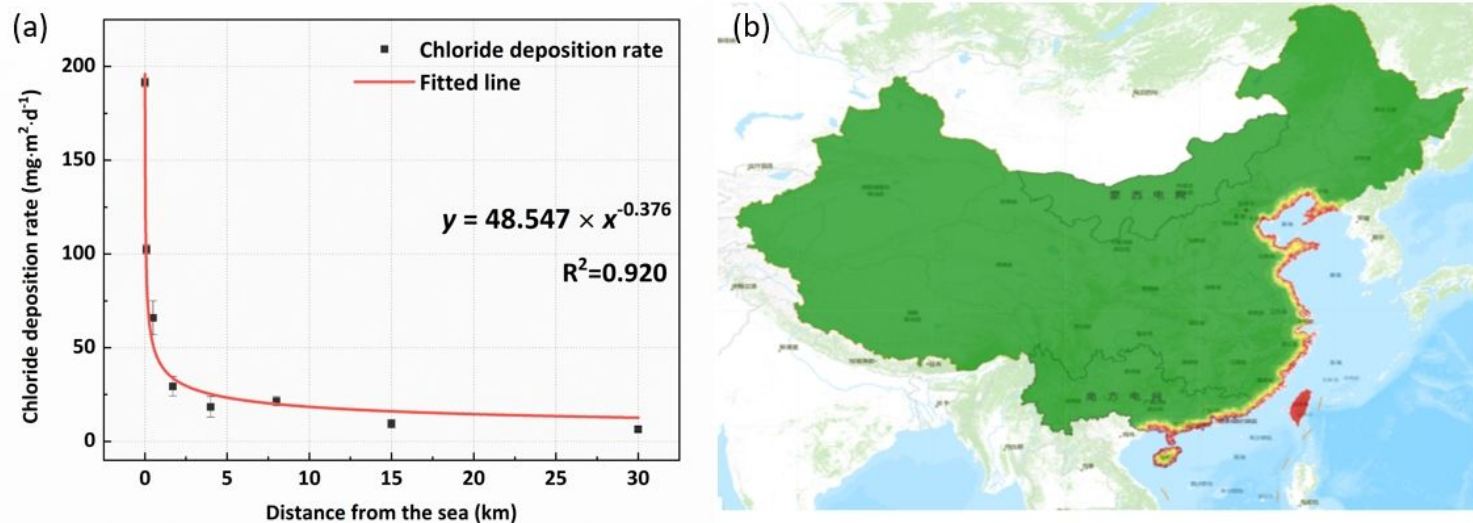Results of corrosion categories of galvanized steel in China according to ISO 9223.

Figure 4

(a) Chloride ion diffusion model in coastal region and (b) Chloride ion distribution map of China.
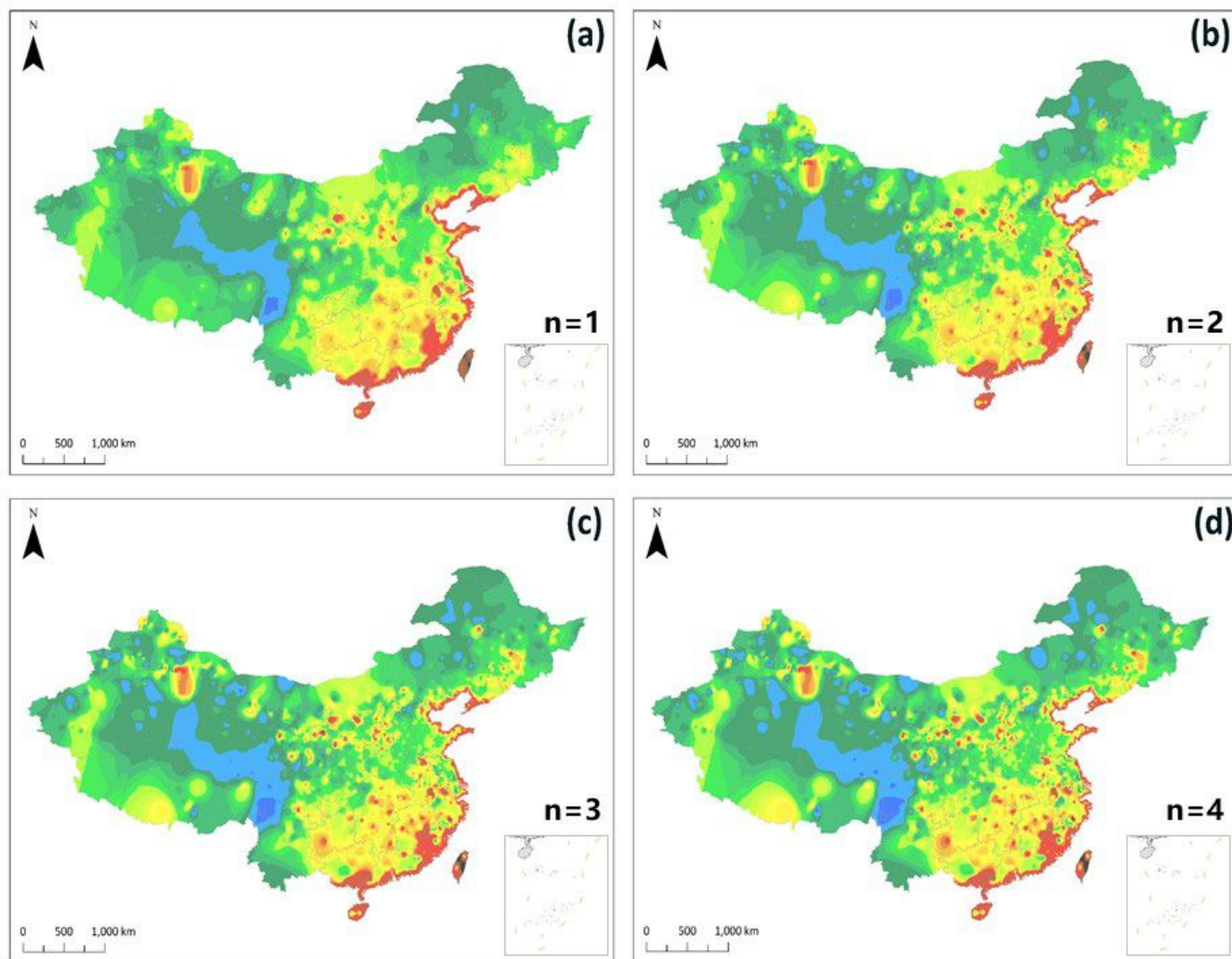
Figure 5

The atmospheric corrosion map of China with powers of 1, 2, 3 and 4.